Supplement of The Cryosphere, 18, 4233–4255, 2024
https://doi.org/10.5194/tc-18-4233-2024-supplement

The Cryosphere Open Access EGU

Supplement of

Feedback mechanisms controlling Antarctic glacial-cycle dynamics simulated with a coupled ice sheet–solid Earth model

Torsten Albrecht et al.

Correspondence to: Torsten Albrecht (albrecht@pik-potsdam.de)

In this supplement, we present further material. It is used in the manuscript to stress the discussed results. In addition (p. 9ff.), we show the impact of further 3D structures, which are based on the investigation of Bagge et al. (2021) and which highlights the sensitivity of Antarctic Ice Sheet response to spatial variability in 3D Earth structures.

List of supplementary figures

List of supplementary videos

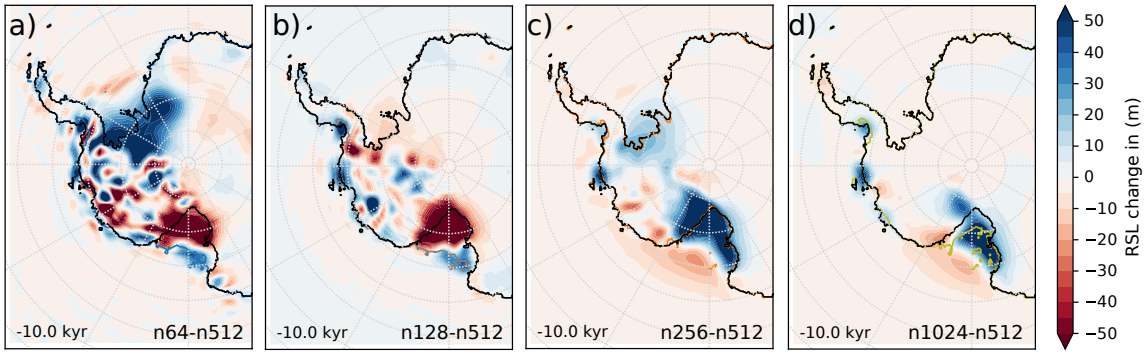

Figure S 1. Difference in RSL between different spatial resolutions at 10 kyr BP in West Antarctica. Black is the GL for the reference resolution n512, colored are the GL for resolution of n64, n128, n256 and n1024, respectively.

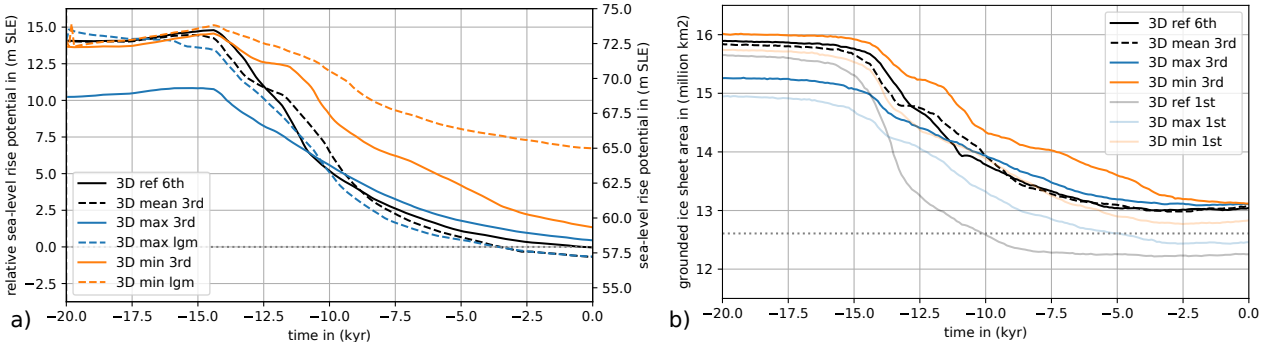

Figure S 2. Sea-level rise potential and grounded ice sheet area over last 20 kyr for different Earth structure configurations. a) Sea-level rise potential in last iteration relative to present-day observations for '3D ref', '3D max' and '3D min' as well as the ice sheet's response for '3D max' and '3D min', when spun-up with the ice load history of the '3D ref' case until 20 kyr BP ('lgm'). Black dashed is the ice sheet response for '3D mean'. b) Grounded ice sheet area in three cases, with transparent lines for first iteration. Dotted horizontal line represents the present-day observation from Bedmap2 (Fretwell et al., 2013), .

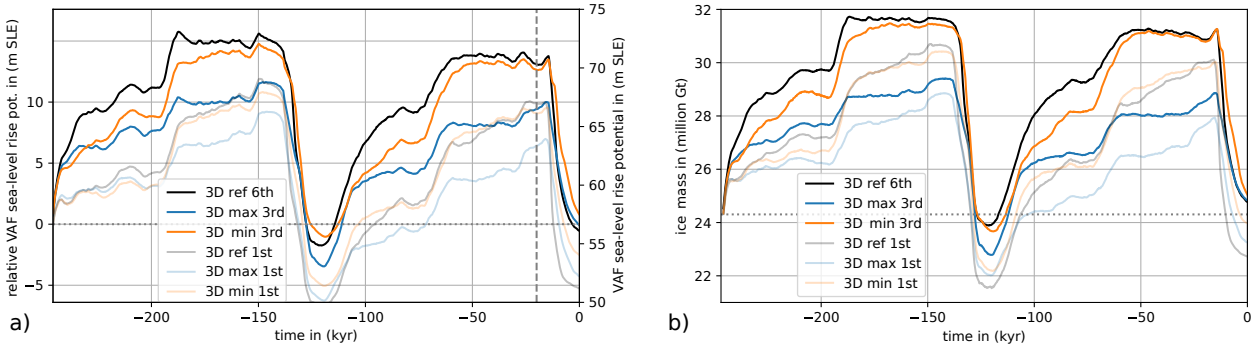

Figure S 3. Antarctic ice volume above flotation and total ice mass over last 246 kyr for different Earth structure configurations. a) Sea-level rise potential from Antarctica in first and last iteration for '3D ref', '3D max' and '3D min' without the corrections applied according to Adhikari et al. (2020). The calculation of the 'volume above flotation' (VAF) follows Eq. 2 in (Goelzer et al., 2020, see Corrigendum). b) Total ice mass in the three cases, with transparent lines for first iteration. Dotted horizontal line represents the present-day observation from Bedmap2 (Fretwell et al., 2013). Initial ice masses are all identical.

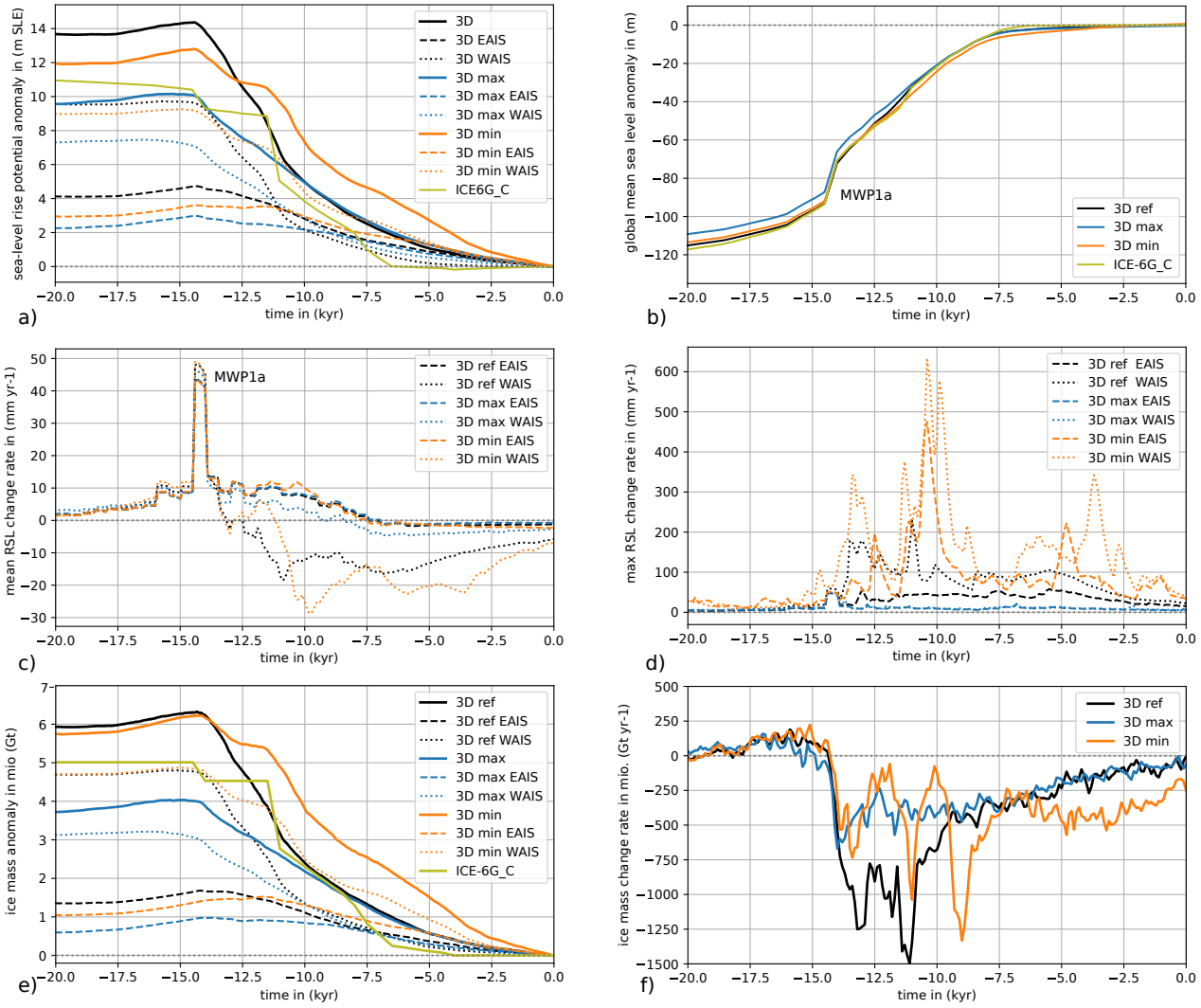

Figure S 4. Anomalies and change rates in sea level metrics over last 20 kyr for different Earth structures. a) Anomaly in SLRP in Antarctica, b) global mean change in relative sea level (RSL), c) mean change rates of RSL, d) maximum change rates of RSL, e) anomaly in Antarctic ice mass and f) change rates in Antarctic ice mass with 100 yr resolution. Blue and orange lines show the response of the ice sheet to '3D max' and '3D min' Earth structure, respectively, black indicates the ice sheet response to '3D ref'. Dashed lines show the response for East Antarctica (75% of the ice-covered area), dotted for West Antarctica (25%). Olive lines show the reconstructions from ICE-6G_C. Melt water pulse 1A is indicated as 'MWP1a'.

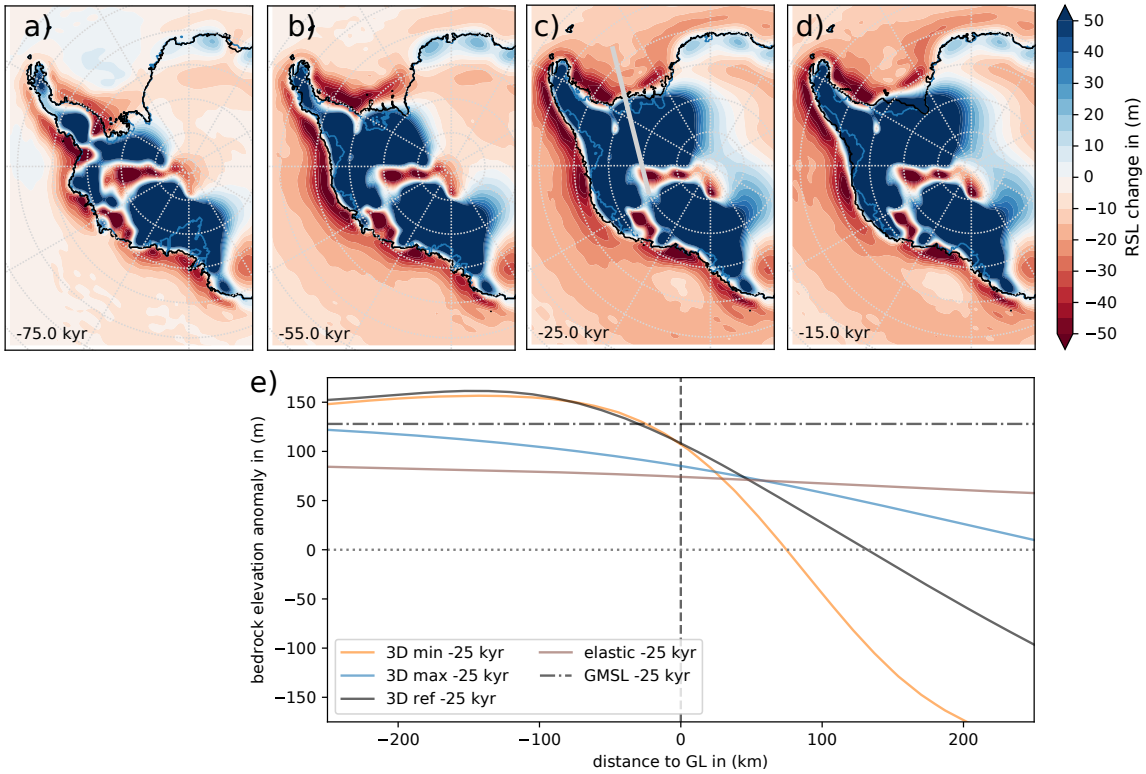

Figure S 5. Difference in RSL between '3D ref' and '3D max' in first iteration at four snapshots during last glaciation , showing peripheral forebulge (red shading) near advancing grounding lines in West Antarctica (black for '3D ref' and blue for '3D max'). Panel e) shows the bedrock elevation change (negative RSL change) along a transect through Ronne Ice Shelf (see grey line in c) with respect to initial bed topography in first iteration at 25 kyr BP, centered around the actual grounding line (GL) position (dashed). Subsidence in the grounded part to the right leads to uplift of a peripheral forebulge in front of the advancing GL (left), in particular for '3D min' case. Positive values indicate a water depth (RSL) lowering, which is a combination of viscoelastic, but also gravitational and rotational effects on top of the barystatic (mean) sea level change (dash-dotted). In the '3D max' case, no forebulge evolves within 250 km distance from the GL, similar to the purely elastic case (brown).

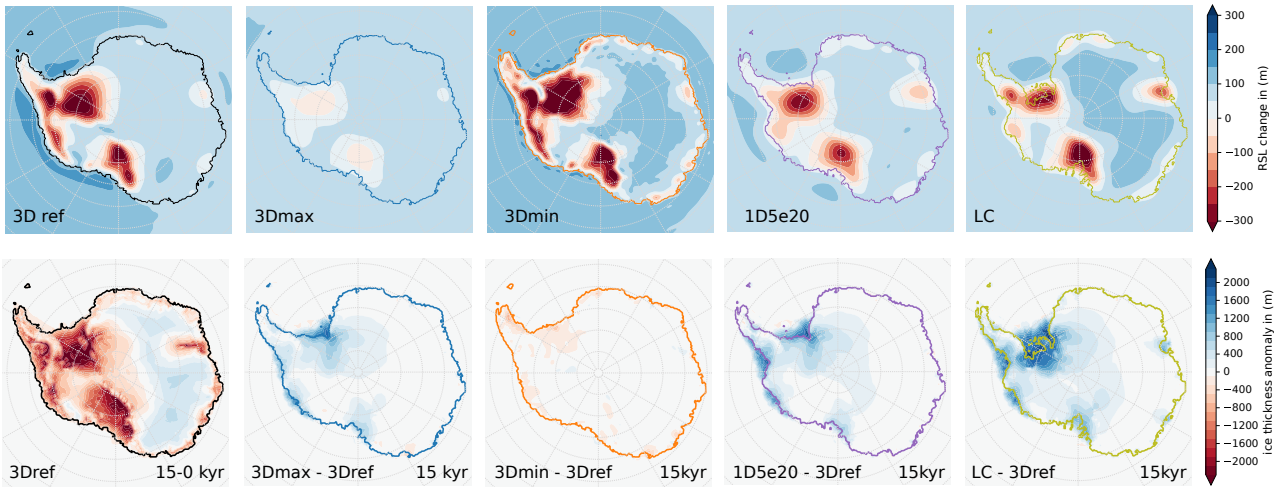

Figure S 6. RSL and ice thickness change since 15 kyr BP, in coupled simulations, for different 3D structures as in Sect. 3.2, and with respect to 1D Earth structure analogous to Lingle-Clark model (LC), as in Sect. 3.3. Corresponding grounding lines at LGM colored. In the lower row, ice thickness anomaly is between LGM (15 kyr BP) and present-day (0 kyr BP) for '3D ref' in the first panel. For the other panels anomaly is between LGM states of different Earth structures.

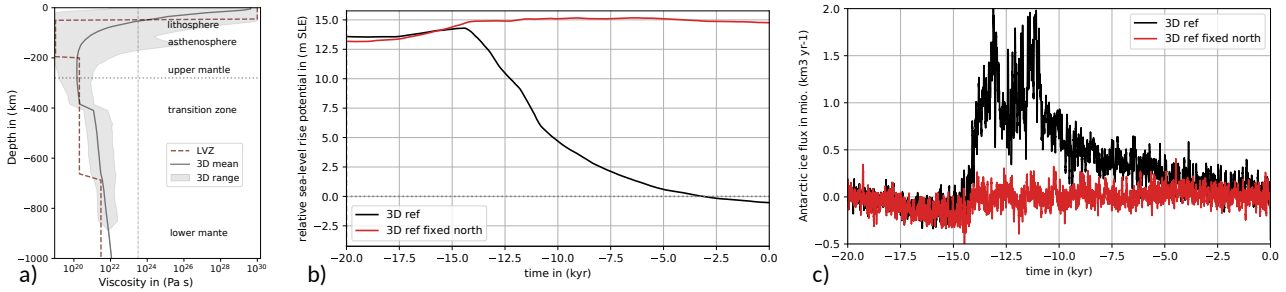

Figure S 7. Global (logarithmic) lateral mean of 3D Earth structures a), sea-level rise potential relative to preset day b) and ice flux over last 20 kyr c) in experiments with evolving (black) and fixed (red) northern hemisphere deglaciations, analogous to Fig. 2b and Fig. 3a in Gomez et al. (2020). Ice flux, as change in total Antarctic ice volume, has been smoothed with a 100-yr running mean. Red dotted line in a) shows 1D Earth structure ('LVZ') used by Gomez et al. (2020). Vertical line denotes threshold of $> 10^{23.5}$ Pa s defining the lithosphere thickness.

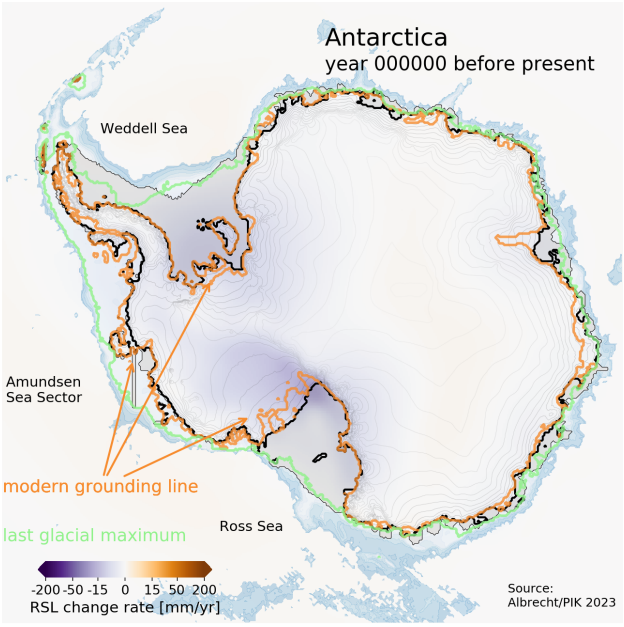

Video S 1: **Change rate of relative sea level (RSL) in Antarctica over the last 25 kyr from a coupled ice sheet–solid Earth model system with reference 3D Earth structure '3D ref'.** Black delineates the grounding line (GL), thin grey the calving front. Green is the GL extent at Last Glacial Maximum, orange the observed present-day GL. Inset shows the global mean sea level change with far-field change rates of up to $50\,\mathrm{mm\,yr^{-1}}$ at around $14.5\,\mathrm{kyr\,BP}$, the Meltwater Pulse 1A. Viscoelastic bedrock uplift in response to marine ice sheet retreat can cause near-field sea level drop of up to -200 $\mathrm{mm\,yr^{-1}}$. Color scale is double logarithmic. Light grey contours indicate ice surface elevation, blue shading indicates the continental shelf up to $1800\,\mathrm{m}$ depth. See Video S 1 at: https://doi.org/10.5446/65479

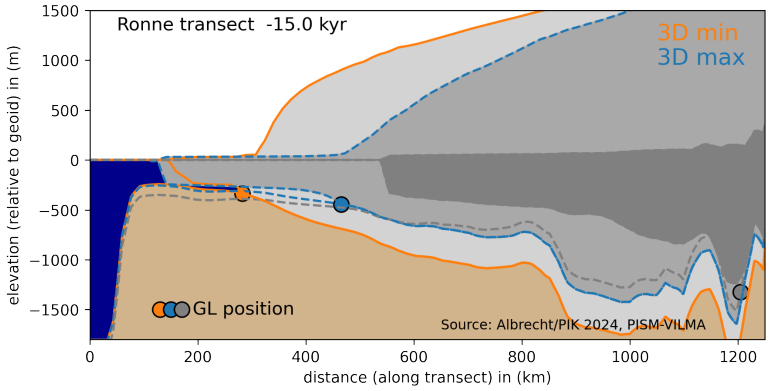

Video S 2: **Change of relative sea level (RSL) along Ronne Ice Shelf transect in Antarctica over the last glacial build-up phase for upper and lower bound of reference 3D Earth structure '3D ref'.** Transect shows bedrock elevation (relative sea level change) and outlines of ice sheet and ice shelf through Ronne embayment from the continental shelf edge to the present-day GL position. The movie shows 0.5 kyr snapshots during glacial build-up between last interglacial (123 kyr BP) and last glacial maximum (15 kyr BP), for the two Antarctic end members of the reference 3D Earth structure, '3D max' and '3D min', in the first iteration (same initial conditions). GL position for '3D min' Earth structure (orange dot) is several 100 km more advanced than for '3D max' (blue dot), likely as a result of a pronounced peripheral forebulge in front of the grounding line. Dark grey shading and dot indicate present-day observed ice sheet configuration and GL position, respectively (cf. Fig. 11b). See Video S 2 at: https://doi.org/10.5446/68302

Sensitivity of Antarctic Ice Sheet response to spatial variability in 3D Earth structures

After we have investigated the Antarctic Ice Sheet response coupled to VILMA for the reference 3D Earth structure '3D ref' (v_0.4_s16) compared to high and low viscosity end member 3D structures '3D min' and '3D max', we will now compare the ice sheet response to different 3D structure classes, obtained from the data compilation in Bagge et al. (2020) following their nomenclature. First, we test for another Class-I-type 3D structure '3D glob' (v_1.0_s16), with larger conversion factor (i.e., activation enthalpy factor) between temperature and viscosity and hence larger lateral variability (see range in Fig. S 10a), but also with a higher global log-mean asthenosphere viscosity and a thicker lithosphere. For this Earth structure, VILMA-standalone simulations provide the best fit to a global dataset of present-day uplift rates (Bagge et al., in prep.). We also consider the Class-II 3D structure '3D ant' (v_1.0_sc06) with the best fit to a subset of these dataset around Antarctica (36 stations) and with a similar lateral variability, but even higher viscosity in the upper mantle (below 210 km) and lower viscosity in the transition zone at the top of the upper mantle (below 410 km depth). For comparison, we apply the intermediate Class-III 3D Earth structure '3D trans' (v_1.0_sc06b) with no strong viscosity jump between the upper mantle and the transition zone. All considered 3D Earth structure classes intersect at the top of the transition zone at a depth of 410 km, and converge in the lower mantle below the transition zone (below 670 km).
They can be distinguished by

- the viscosity in the upper mantle and transition zone, determined by the radial viscosity profile
- the lithosphere thickness, determined by the conversion factor and
- the lateral variablity, determined by the conversion factor.

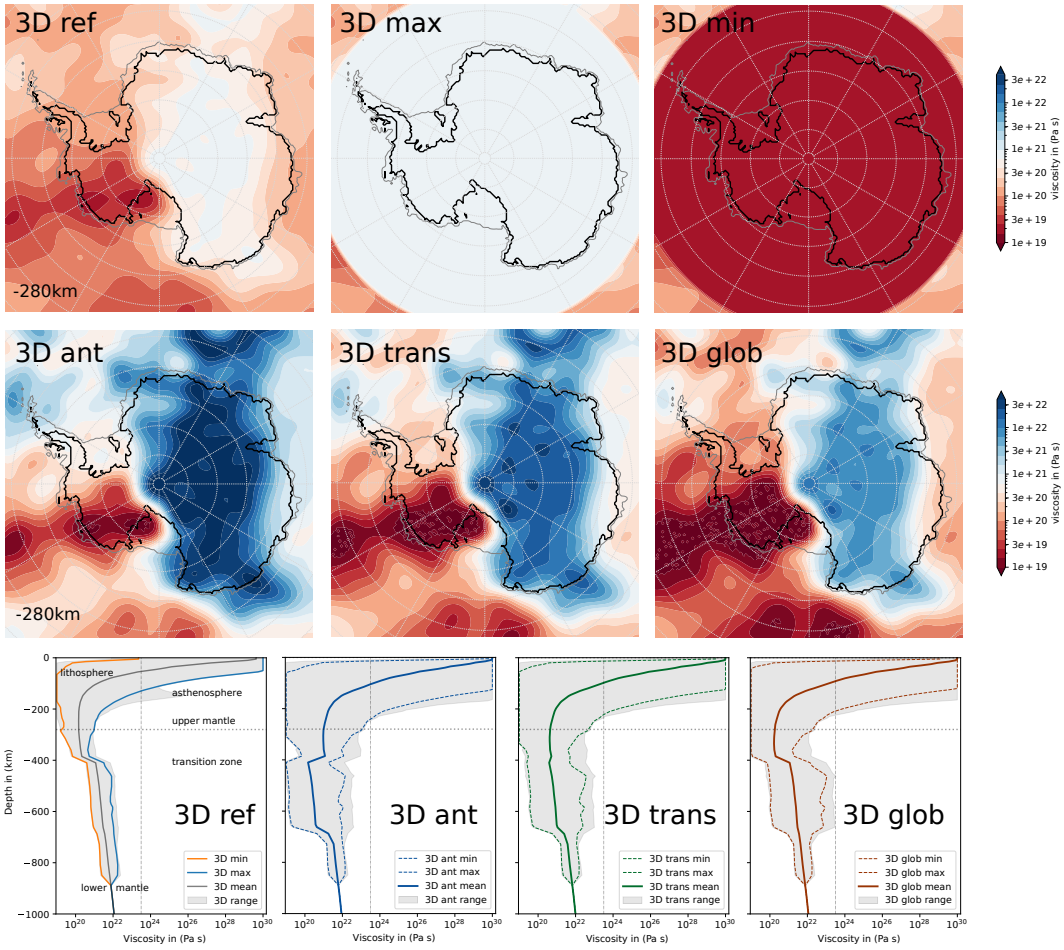

Figure S 8. Earth structures underneath Antarctica with upper-mantle viscosity shown at 280 km depth for the six different 3D structures considered. Vertical profiles show global range, logarithmic mean and minimum and maximum values in Antarctic domain for four of the 3D Earth structures. Note that colorbar range differs from that in Fig. 5b.

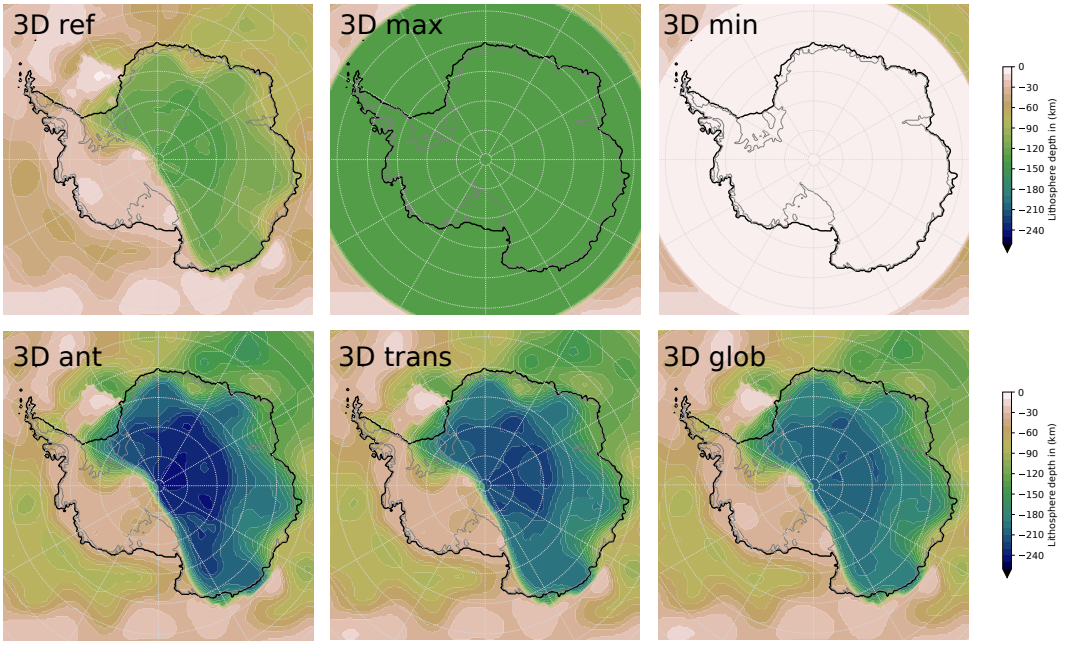

Figure S 9. Lithosphere thickness underneath Antarctica for the six different 3D structures considered. Note that colorbar range differs from Fig. 5c.

In our coupled simulations, the range of deglacial response of the Antarctic Ice Sheet SLRP to variation in 3D Earth structure classes is comparably small, with largest differences of about 3 m SLE at LGM (Fig. S 10c) obtained for '3D ref', which also shows the largest SLRP in Antarctica. Among the considered classes, '3D ref' has the lowest global mean upper-mantle viscosity, the thinnest lithosphere (Fig S 9) and the smallest global range (lateral variability, factor 0.4). For larger lateral variability (factor 1.0) we find for increasing upper mantle viscosity and decreasing lower mantle viscosity (s16, sc06b, sc06, see Fig. S 10a) slightly decreasing SLRP at LGM. The trajectories of deglacial ice loss over the last 15 kyr is similar in all classes, converging after 10 kyr BP in the coupled simulations (Fig. S 10c). Already in the first iteration, the three classes with similar lateral variability and lithosphere thickness ('3D glob', '3D trans' and '3D ant') show a very similar ice volume (SLRP) response since LGM, while for '3D ref' the LGM ice volume is larger and the present-day ice volume is smaller (compare transparent lines in Fig. S 10c). Also, the convergence rate for the iterative optimization of present-day bed topography is lowest for '3D ref'. The present-day anomaly is alternating with each iteration and it takes 6 iterations instead of 3 to reach an RMSE below 10 m (cf. Fig. 4 and Fig. S 10b). Likely, this effect is caused by the thin lithosphere, and is even more pronounced for the lower end '3D min' (Fig. 3c).

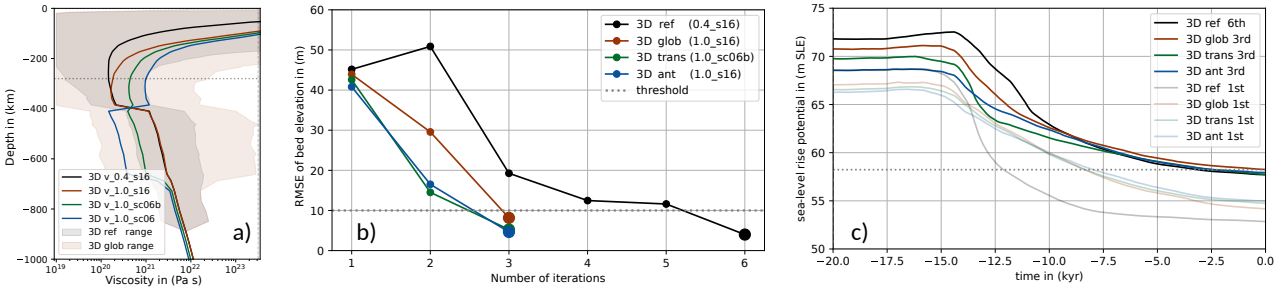

Figure S 10. Global (logarithmic) lateral mean viscosity of 3D Earth structures a), RSL convergence at present b) and corresponding SLRP from Antarctica c) over the last 20 kyr for different 3D Earth model configurations. Black color indicates the reference 3D Earth structure '3D ref' (v_0.4_s16, Class-I), red-brown a similar 3D structure but with more lateral variability '3D glob' (v_1.0_s16, Class-I), green an intermediate 3D structure '3D trans' (v_1.0_sc06b, Class-III) and dark-blue the 3D structure that has an opposite viscosity jump between the upper mantle and the transition zone '3D ant' (v_1.0_sc06, Class-II). In a) the range between global mininum and maximum viscosity for '3D ref' is shaded in grey, and redish for the '3D glob' Earth structure with larger lateral variability and thicker lithosphere. In c) for comparison, first iteration results are shown in transparent colors.

References

Adhikari, S., Ivins, E. R., Larour, E., Caron, L., and Seroussi, H.: A kinematic formalism for tracking ice–ocean mass exchange on the earth's surface and estimating sea-level change, The Cryosphere, 14, 2819–2833, https://doi.org/10.5194/tc-14-2819-2020, 2020.

Bagge, M., Klemann, V., Steinberger, B., Latinovic, M., and Thomas, M.: 3D Earth structures for glacial-isostatic adjustment models, V. 1.0, GFZ Data Services, https://doi.org/10.5880/GFZ.1.3.2020.004, 2020.

Bagge, M., Klemann, V., Steinberger, B., Latinović, M., and Thomas, M.: Glacial-Isostatic Adjustment Models Using Geodynamically Constrained 3D Earth Structures, Geochemistry, Geophysics, Geosystems, 22, e2021GC009 853, https://doi.org/10.1029/2021GC009853, 2021.

Bagge, M., Boergens, E., Balidakis, K., Klemann, V., and Dobslaw, H.: A validation method for modelled present-day GIA uplift rates against space geodetic data, Solid Earth, in prep.

Fretwell, P., Pritchard, H. D., Vaughan, D. G., Bamber, J. L., Barrand, N. E., Bell, R., Bianchi, C., Bingham, R. G., Blankenship, D. D., Casassa, G., Catania, G., Callens, D., Conway, H., Cook, A. J., Corr, H. F. J., Damaske, D., Damm, V., Ferraccioli, F., Forsberg, R., Fujita, S., Gim, Y., Gogineni, P., Griggs, J. A., Hindmarsh, R. C. A., Holmlund, P., Holt, J. W., Jacobel, R. W., Jenkins, A., Jokat, W., Jordan, T., King, E. C., Kohler, J., Krabill, W., Riger-Kusk, M., Langley, K. A., Leitchenkov, G., Leuschen, C., Luyendyk, B. P., Matsuoka, K., Mouginot, J., Nitsche, F. O., Nogi, Y., Nost, O. A., Popov, S. V., Rignot, E., Rippin, D. M., Rivera, A., Roberts, J., Ross, N., Siegert, M. J., Smith, A. M., Steinhage, D., Studinger, M., Sun, B., Tinto, B. K., Welch, B. C., Wilson, D., Young, D. A., Xiangbin, C., and Zirizzotti, A.: Bedmap2: improved ice bed, surface and thickness datasets for Antarctica, The Cryosphere, 7, 375–393, https://doi.org/10.5194/tc-7-375-2013, 2013.

Goelzer, H., Coulon, V., Pattyn, F., De Boer, B., and Van De Wal, R.: Brief communication: On calculating the sea-level contribution in marine ice-sheet models, The Cryosphere, 14, 833–840, https://doi.org/10.5194/tc-14-833-2020, 2020.

Gomez, N., Weber, M. E., Clark, P. U., Mitrovica, J. X., and Han, H. K.: Antarctic ice dynamics amplified by Northern Hemisphere sea-level forcing, Nature, 587, 600–604, https://doi.org/10.1038/s41586-020-2916-2, 2020.